Matter and Radiation at Extremes

RESEARCH ARTICLE | FEBRUARY 29 2024

Self-consistent and precise measurement of time-dependent radiative albedo of gold based on specially symmetrical triple-cavity *Hohlraum*

Zhiyu Zhang ; Yang Zhao; Xiaoying Han; Liling Li ; Bo Qing; Lifei Hou; Yulong Li; YuXue Zhang ; Huan Zhang; Xiangming Liu; Bo Deng; Gang Xiong ; Min Lv ; Tuo Zhu ; Chengwu Huang; Tianming Song ; Yan Zhao; Yingjie Li; Lu Zhang ; Xufei Xie ; Jiyan Zhang ; Jiamin Yang

Matter Radiat. Extremes 9, 037601 (2024)
https://doi.org/10.1063/5.0177038

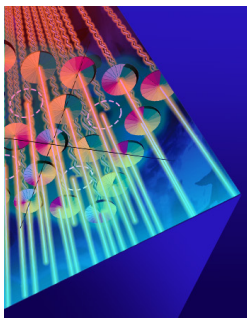

Matter and Radiation at Extremes

RESEARCH ARTICLE

pubs.aip.org/aip/mre

Self-consistent and precise measurement of time-dependent radiative albedo of gold based on specially symmetrical triple-cavity *Hohlraum*

Cite as: Matter Radiat. Extremes 9, 037601 (2024); doi: 10.1063/5.0177038
Submitted: 19 September 2023 • Accepted: 1 February 2024 •
Published Online: 29 February 2024

Zhiyu Zhang,[1,2] Yang Zhao,[1,2] Xiaoying Han,[3] Liling Li,[1,2] Bo Qing,[1,2] Lifei Hou,[1,2] Yulong Li[1,2] YuXue Zhang,[1,2] Huan Zhang,[1,2] Xiangming Liu,[1,2] Bo Deng,[1,2] Gang Xiong,[1,2] Min Lv,[1,2] Tuo Zhu,[1,2] Chengwu Huang,[1,2] Tianming Song,[1,2] Yan Zhao,[1,2] Yingjie Li,[1,2] Lu Zhang,[1,2] Xufei Xie,[1,2] Jiyan Zhang,[1,2,a)] and Jiamin Yang[1,2,b)]

AFFILIATIONS

[1] Laser Fusion Research Center, China Academy of Engineering Physics, Mianyang 621900, China
[2] National Key Laboratory of Plasma Physcis, Mianyang 621900, China
[3] Institute of Applied Physics and Computational Mathematics, Beijing 100088, China

[a)] **Electronic mail:** zhangjiyanzjy@163.com
[b)] **Author to whom correspondence should be addressed:** yjm70018@sina.cn

ABSTRACT

A self-consistent and precise method to determine the time-dependent radiative albedo, i.e., the ratio of the reemission flux to the incident flux, for an indirect-drive inertial confinement fusion *Hohlraum* wall material is proposed. A specially designed symmetrical triple-cavity gold *Hohlraum* is used to create approximately constant and near-equilibrium uniform radiation with a peak temperature of 160 eV. The incident flux at the secondary cavity waist is obtained from flux balance analysis and from the shock velocity of a standard sample. The results agree well owing to the symmetrical radiation in the secondary cavity. A self-consistent and precise time-dependent radiative albedo is deduced from the reliable reemission flux and the incident flux, and the result from the shock velocity is found to have a smaller uncertainty than that from the multi-angle flux balance analysis, and also to agree well with the result of a simulation using the HYADES opacity.

Laser indirect-drive inertial confinement fusion (ICF), in which high power laser is deposited in a *Hohlraum* made from high-*Z* material and then used to compress the fuel to high temperature and density indirectly, is one of the pathways most likely to generate clean energy in the future.[1–3] Although recent ICF experiments have demonstrated fusion ignition,[4] with more than 3 MJ of fusion energy being released for a delivered laser energy of 2.05 MJ, many physical processes in ICF, such as the degree of radiation uniformity in the *Hohlraum* and the subsequent drive asymmetry are not fully understood, and much work remains to be done.[5–15] In an indirect-drive ICF *Hohlraum*, the incident beam power is first converted into x-ray radiation at a few interaction spots, and this radiation is then continuously absorbed and partially reemitted by the wall. Therefore, the radiative albedo, i.e., the ratio of the reemission x-ray flux to the incident x-ray flux, is an important factor in attempts to improve radiation uniformity in the *Hohlraum* and thus reduce capsule asymmetries, because a higher albedo reduces the discrepancy in brightness between the spots and the un-irradiated region.[16] In these processes, the x-ray conversion efficiency from lasers is about 70%–80%. However, only 10%–20% of the laser energy will be finally coupled to the capsule. Most of the energy is absorbed by the *Hohlraum* walls, about 40% of the laser energy or about 60% of the x-ray energy.[2] Therefore, a higher albedo also helps to reduce the energy absorbed by the *Hohlraum* walls and thus improve the efficiency of energy coupling to the capsule. The radiative albedo of the *Hohlraum* depends on the process of interaction

between the radiative source and the wall material, which is related to the radiative opacity of the material. Owing to the complexity of both the interaction and the opacity of the high-Z material, it is difficult to give an exact analytical expression for the radiative albedo or the reemission flux. There have been some previous investigations of reemission from laser-heated *Hohlraums*.[17–19] However, owing to limitations on direct measurements of the incident flux, it is difficult to determine the radiative albedo. Jones *et al.*[16] performed a measurements of albedo for gold at peak temperatures of 70 and 100 eV and then tested different opacity models. In their experiment, a filtered x-ray diode array called DANTE was used to measure the flux of the primary *Hohlraum* and a double *Hohlraum* from a fixed angle in different shots. The acquisition of the albedo from a flux balance analysis relies on some corrections from the view-factor method and the angular dependence, and the radiative temperature obtained is relatively low. To improve the accuracy of albedo determination, some other relevant physical quantities need to be introduced to further constrain the incident flux, such as the shock wave velocity. Previous studies have been focused on inverting the peak value of the radiative source based on the average shock wave velocity. Studies of the time evolution of the incident flux based on the shock wave velocity have been rare. Also, to increase the radiation temperature, a triple-cavity *Hohlraum* is a potential method, and this has been used to generate clean radiation sources as well as for radiation transport studies.[1,20]

In this work, we present a self-consistent and precise method to determine the time-dependent radiative albedo with a combination of x-ray flux and shock velocity measurements. A specially designed symmetrical triple-cavity *Hohlraum* is used to create approximately constant and near-equilibrium radiation with a peak temperature of 160 eV. The multi-angle radiative flux of the primary cavity, the reliable x-ray reemission flux from the secondary cavity wall, and the shock velocity evolution in a standard sample (aluminum–quartz) are all measured and are used to provide a self-consistent incident x-ray flux onto the secondary cavity wall with two methods. Finally, the precise time-dependent radiative albedo is obtained from the reliable reemission flux and the incident flux, and this is then compared with the simulated results for different opacity parameters.

The experiment was performed on the SG-100 kJ high-power laser facility[21,22] with a specially designed triple-cavity gold *Hohlraum*, consisting of two primary cavities with diameters of 2.4 mm and lengths of 2.45 mm and one secondary cavity with a diameter of 2.4 mm and a length of 2.0 mm, as shown in Fig. 1(a). Forty-eight shaped laser beams, each with a pulse duration of 2 ns as shown in Fig. 1(c) and a wavelength of 0.351 μm, were injected into the two primary cavities from the laser entrance holes (LEHs) with diameters of 1.2 mm. The x-rays generated in the primary cavities were transported into the secondary cavity through connecting holes with diameters of 1.2 mm. An approximately constant radiation field in the secondary cavity was created, since the laser pulse was well shaped. Moreover, the special geometric design of the triple-cavity *Hohlraum* with the laser spots shielded created near-equilibrium radiation with much reduced M-band influence in the secondary cavity. There were two diagnostic holes (DHs) located at the waist of the secondary cavity: a space-resolved flux detector (SRFD),[23] whose field of view with a diameter of 400 μm was smaller than the size of the DH, was used to measure the reemission flux of the secondary cavity, $F_{2,\mathrm{r}}(t)$, from one DH with a diameter of 800 μm, and an imaging velocity interferometer system for any reflector (VISAR)[24] was used to measure the shock velocity $D(t)$ in standard samples (aluminum–quartz) with thicknesses of 40 and 100 μm, respectively, adhered on the other square-shaped DH of size 800 × 1000 μm^2. The locations of the DHs were so designed that the blowoff plasma from the aluminum sample attached to one of the DHs would not influence the line of sight from the other DH for the reemission flux measurement. Owing to this special symmetrical design, both the

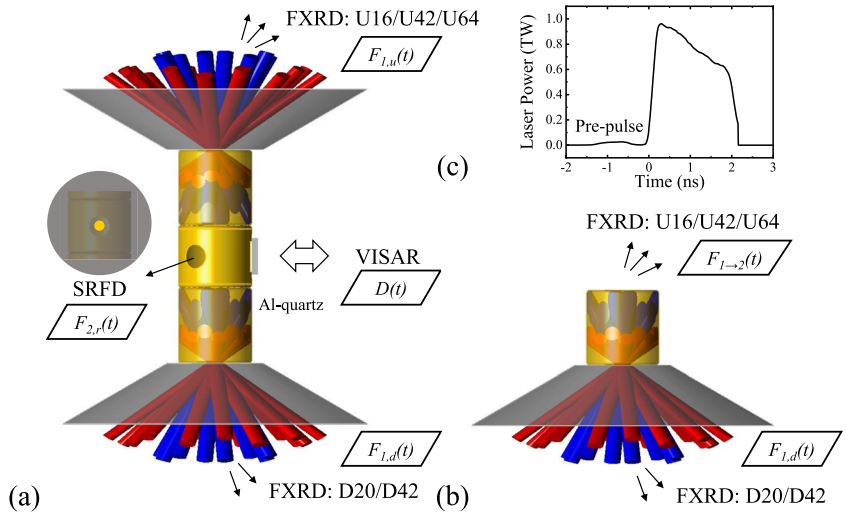

FIG. 1. (a) and (b) Schematic of *Hohlraum* and experimental setup. To suppress movement of the Au bubble, the *Hohlraum* is filled with neopentane (C_5H_{12}) gas at about 0.4 atm and has thin (0.5 μm) plastic membranes covering the laser entrance holes (LEHs) and diagnostic holes (DHs). (c) Laser power per beam. There is a small prepulse with duration of 1.0 ns arriving 0.5 ns before the main pulse to heat the membranes attached to the LEHs, causing them to expand and evaporate.

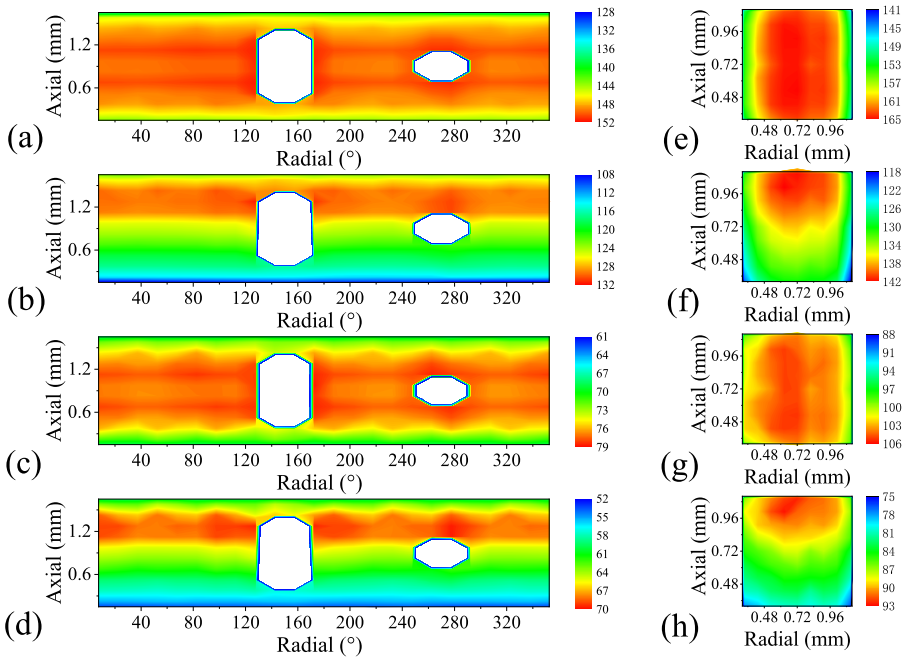

FIG. 2. (a)–(d) Simulated radiative temperature distribution of the secondary cavity wall with laser injection from (a) two sides and (b) one side at high temperature, and (c) two sides and (d) one side at low temperature. (e)–(h) Simulated incident radiative temperature distribution to the standard sample at the secondary cavity waist with laser injection from (e) two sides and (f) one side at high temperature, and (g) two sides and (h) one side at low temperature.

radiative temperature and homogenization of the secondary cavity were improved. This was validated by a view factor code IRAD3D, which had been verified by a cross-check against the widely used code VISRAD.[25] Simulations with laser injection from two sides or only one side were performed, and the reemission radiative temperature distribution of the secondary cavity wall and the incident radiative temperature distribution to the standard sample at the secondary cavity waist were obtained and are plotted in Fig. 2. The radiation in this triple-cavity *Hohlraum* with laser injection from two sides was clearly more symmetrical than that in previous work for the whole time (from low temperature to high temperature). Therefore, the measurement of the reemission flux at the secondary cavity waist was more reliable. Moreover, the simulation results also indicated that the discrepancy between the reemission radiative temperature at the cavity waist and the mean radiative temperature of the secondary cavity wall was small (~2 eV), and so the flux balance analysis in the secondary cavity used below was more reliable.

Five flat-response x-ray diode (FXRD) detectors[26,27] were used to measure the time-resolved x-ray flux intensities of the primary cavity from the LEHs: $F_{1,\mathrm{u}}(t)$ at viewing angles relative to the cavity axis of 16° (U16), 42° (U42), and 64° (U64) from the upper hemisphere of the target chamber; $F_{1,\mathrm{d}}(t)$ at 42° (D42) and 20° (D20) from the lower hemisphere. These FXRD detectors can provide a flat response in the 0.1–4 keV photon energy range because of their special cathode and filter design and have been absolutely calibrated at he Beijing Synchrotron Radiation Facility. In a separate shot, a one-cavity *Hohlraum* with only the primary cavity and injection of 24 laser beams from the lower LEH as shown in Fig. 1(b) was used to characterize the radiation flux entering the secondary cavity. In that shot, the U16/U42/U64 FXRD detectors were used to measure the radiation flux $F_{1\to2}(t)$ from the upper connection hole, which can be used to represent the flux transported into the secondary cavity in the triple-cavity shots. Preliminary results for the incident flux and radiative albedo can first be obtained from the reliable multi-angle flux balance analysis in the secondary cavity. Then, a more credible incident flux can be deduced on the basis of the relationship between the incident flux and the drive shock velocity. Finally, a self-consistent and then precise time-dependent radiative albedo is obtained by comparing the results from these two methods.

As shown in Fig. 3(a), the time-dependent radiation temperature, which represents the radiation flux measured from the lower LEH by the D20/D42 FXRD detectors, $F_{1,\mathrm{d}}(t)$, is almost the same in both triple-cavity and one-cavity *Hohlraum* shots. For simplicity, the radiation flux is represented by the corresponding radiation temperature in the following. The radiation fluxes measured by the U16/U42/U64 FXRD detectors are presented in Fig. 3(b). The solid and dashed lines represent the results from the triple-cavity *Hohlraum* shots with injection of 48 laser beams, $F_{1,\mathrm{u}}(t)$, and the dotted line represents the result from the one-cavity *Hohlraum* shot with injection of just the 24 lower laser beams, $F_{1\to2}(t)$. The consistency of the flux measured from the LEH with laser injection indicates the reproducibility of the experiments and the flux consistency between different *Hohlraum* shots. Therefore, the flux measured by the upper FXRD detectors in the one-cavity *Hohlraum* shot, $F_{1\to2}(t)$, can be used to represent the flux transported into the secondary cavity in the triple-cavity *Hohlraum* shot, since the reflux

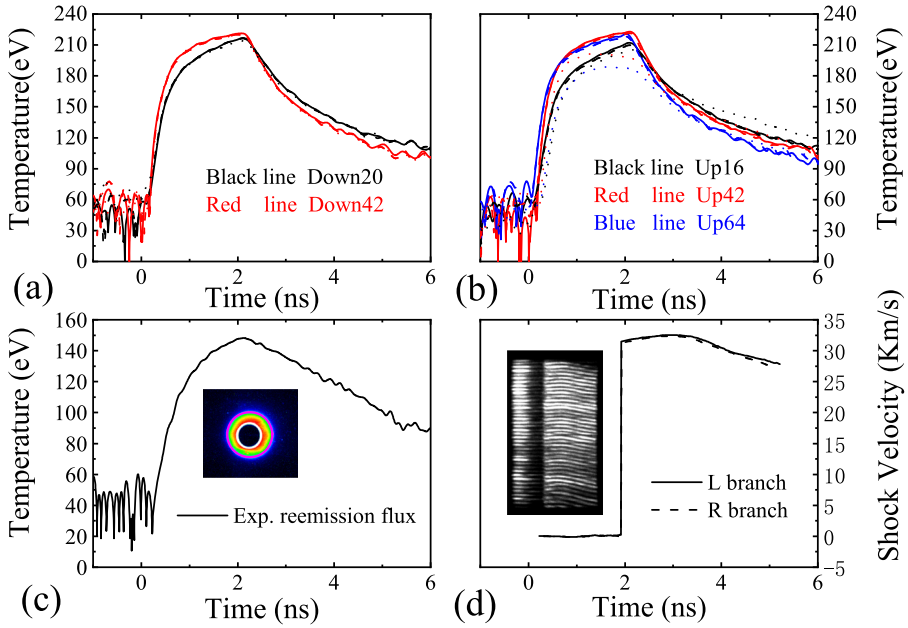

FIG. 3. Radiation fluxes measured by (a) D20/U42 FXRD detectors and (b) U16/U42/U64 FXRD detectors. The solid and dashed lines represent the results from the three-cavity *Hohlraum* shots, and the dotted line represents the result from the one-cavity *Hohlraum* shot. (c) Experimental reemission flux from the secondary cavity. It can be seen that the SRFD (whose field of view is represented by the white circle) is aimed at the center of the diagnostic hole (magenta circle), where the reemission is relatively uniform. (d) Shock velocity of aluminum–quartz sample. The inset is an example of an original interference fringe image measured by VISAR.

to the primary cavity is small. As shown in Fig. 3(b), this flux $F_{1\to2}(t)$ is smaller than the flux from the LEH with laser injection, a possible reason being the presence of cold plasma at the front of the bubble[28] or the larger closure of the connecting hole without laser injection. Moreover, the time profiles of the fluxes measured from different angles behave differently after the rising edge (1–2 ns), namely, rising, decreasing smoothly, or remaining approximately constant for the 16°, 42°, and 64° angles, respectively, confirming the importance of multi-angle measurement. Fortunately, there is no obvious attenuation with time for the total flux transported into the secondary cavity, considering the angular distribution of the measured multi-angle flux, which is a requirement for the validity of the scaling relationship between the drive temperature and the shock velocity.

The reemission flux from the secondary cavity measured by the SRFD and its field of view are presented in Fig. 3(c). The field of view is limited by the pinhole located in the front of the SRFD to 400 μm diameter and is aimed at the center of the DH with a diameter of 800 μm. Both the SRFD image and the radiation hydrodynamic simulations reveal that the DH closure is smaller than 150 μm during laser injection, and the reemission in the view field is almost uniform. Therefore, the measured reemission flux will not be disturbed by the DH closure or by background radiation from other sources. The flux keeps rising during the first 2.0 ns when the laser beams were turned on. The background flux was also measured with a non-DH *Hohlraum* and can be neglected compared with the reemission flux. The reemission flux in 1.6–4 keV was also measured by several M-band x-ray diodes (MXRDs)[29] at the same angles of the SRFD. Since MXRDs almost have no signals when compared with that of the SRFD, it means that the high-energy photon emissions such as the M-band x-rays of Au emissions have been inhibited, and the x-ray flux satisfies the assumption of a Planckian Au emission.

A dual-sensitivity VISAR was used to measure the shock velocity of a standard sample (aluminum–quartz) adhered on one DH of the secondary cavity. The x-rays in the secondary cavity ablate the aluminum sample and drive shock waves continuously. When the shock wave propagates in the aluminum layer, the probe laser light will be reflected on the aluminum–quartz interface and there is no fringe shift in the interference image. When the shock wave enters the quartz layer, an impedance-matched transparent window for aluminum, the probe laser will be reflected at the shock front if the intensity of the shock wave is strong enough, and the interference fringes will change with the shock velocity. An original interference fringe image measured by the VISAR is shown in Fig. 3(d). The intensity of the interference fringe weakens during 0–1.9 ns because of the preheating effect due to the high-energy x-ray tail of the radiation. Fortunately, the transparency of quartz is not influenced by the preheating effect, because the high-energy x-rays still exist after 1.9 ns, but the interference fringe brightens. This indicates that the preheating effect influences only the reflectivity of aluminum and not the transparency of quartz, and so the propagation of the shock wave in quartz can be measured without disturbance. The shock velocities extracted from the fringes are also plotted in Fig. 3(d). The results for two branches with different etalons are almost the same. The shock wave propagates in the

aluminum during 0–1.9 ns, and so it cannot be measured by the VISAR during this time. The shock velocity keeps rising slightly (~32 km/s) during 1.9–3.3 ns and then decreases with time. As mentioned above, the incident flux of the sample drives shock waves continuously, and so a shock will catch up with its predecessor and will be attenuated unless the drive flux keeps rising. However, considering the delay between the measurement of the shock velocity and the laser injection, the incident flux on the sample probably keeps rising during laser injection. Moreover, the measured shock velocity can be verified by comparing its integral $\int_0^{6\text{ns}} D(t)\,dt$ with the thickness of the quartz, where the discrepancy is found to be smaller than 2%.

Preliminary results for the time-dependent radiative albedo and the incident flux at the secondary cavity waist can be deduced from a flux balance analysis with multi-angle flux measurement.[3] Considering the different fluxes flowing in and out of unit area of the wall surface in the secondary cavity, the incident flux F_i can be expressed as

$$F_\text{i} = \frac{F_\text{s}A_\text{ch}}{A_\text{t}} + \frac{F_{\text{r-Au}}A_{wall}}{A_\text{t}} + \frac{F_{\text{r-Al}}A_{\text{dh-Al}}}{A_\text{t}},$$

where F_s represents the external heating source, A_ch is area of connecting holes, $F_{\text{r-Au}}$ is the reemission flux of Au, A_{wall} is the area of the Au surface, $F_{\text{r-Al}}$ is the reemission flux of Al, $A_{\text{dh-Al}}$ is the area of the DH for the Al sample, and $A_\text{t} = A_{wall} + A_\text{ch} + A_{\text{dh-flux}} + A_{\text{dh-Al}}$ is the total area. Therefore, the radiative albedo of gold, $\alpha = F_\text{r}/F_\text{i}$, can be expressed as

$$\frac{1}{\alpha_\text{Au}} = \frac{A_{wall} + A_{\text{dh-Al}}\alpha_\text{Al}/\alpha_\text{Au}}{\alpha_\text{t}} + \frac{A_\text{ch}}{A_\text{t}}\frac{F_\text{s}}{F_{\text{r-Au}}} \approx \frac{A_{wall}}{A_\text{t}} + \frac{A_\text{ch}}{A_\text{t}}\frac{F_\text{s}}{F_{\text{r-Au}}},$$

where the $A_{\text{dh-Al}}\alpha_\text{Al}/\alpha_\text{Au}$ can be neglected since A_{wall} is about 25 times as large as $A_{\text{dh-Al}}$ and α_Au is also several times as large as α_Al.

The external source flux for the secondary cavity, $F_\text{s}A_\text{ch}$ can be deduced from the measured multi-angle fluxes $F_{1\to2}(t)$ plotted in Fig. 3(b). The reemission flux of the secondary cavity, $F_{\text{r-Au}}$, has been measured perpendicularly and is plotted in Fig. 3(c). Therefore, the time-dependent radiative albedo and the incident flux of the secondary cavity waist can be deduced from the above flux balance analysis and are plotted in Fig. 4(a) (blue dashed line for α_0 and red dashed line for T_{in0}). It must be said that there is a strong hypothesis that the radiation is uniform in the secondary cavity. Fortunately, the view factor simulation shown in Fig. 2 indicates that the discrepancy between the reemission temperature from the DH and the equivalent average temperature of the whole secondary cavity is small enough that the hypothesis is acceptable. Therefore, the uncertainty of the radiative albedo α_0 from the flux balance analysis is mainly determined by the uncertainties in $F_{\text{r-Au}}$ and F_s, which are 10% and 20%, respectively. Considering the acceptable roughness of the flux balance method, the uncertainty in the radiative albedo α_0 is about 20%.

Alternatively, the incident flux at the secondary cavity waist can be obtained from the measured shock velocity of the standard sample (aluminum–quartz). The incident flux ablates the standard sample and launches shock waves. A shock will catch up with its predecessor, because the incident flux keeps rising during laser injection. Therefore, the measured shock velocity is closely linked to the drive source. Under ideal conditions,[30] the relationship between the shock velocity and the drive source can be represented by an empirical scaling $v_\text{s}\ [\mu\text{m/ns}] = 0.0046T\ [\text{eV}]^{1.75}$, which indicates that a small change of the drive source will lead to a relative larger variation in the shock velocity. The sensitivity of the shock velocity to the input source is also examined by modifying the source flux rising edge, peak temperature, and falling edge in a hydrodynamic simulation implemented by MULTI,[31] and the results indicate that the shock velocity is sensitive to the profile of the source flux. Using the incident flux from the flux analysis as input, the shock velocity of the standard sample whose parameters have been validated in equation-of-state experiments[32–35] is simulated. As shown in Fig. 4(b), there is a considerable discrepancy between the evolution of the simulated (red dotted line for D_{sim0}) and experimental (olive dash-dotted and dark cyan dashed lines for D_{exp}) shock

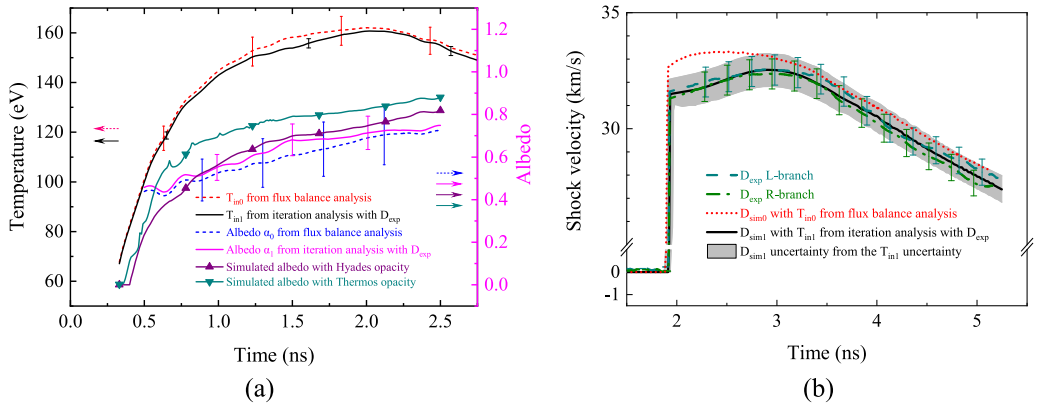

FIG. 4. (a) Incident flux and radiative albedo of secondary cavity from the multi-angle flux balance analysis (T_{in0}, α_0) and from an iterative analysis with the experimental shock velocity (T_{in1}, α_1), together with simulated radiative albedo for different opacity parameters. (b) Comparison between experimental shock velocity and simulation results with incident flux T_{in0} from flux balance analysis and T_{in1} from iterative analysis with D_{exp}.

velocities. The simulated result D_{sim0} is larger than the experimental data. Considering the delay between the drive source and the measured shock velocity, the intensity of the incident flux should be revised during 1.0–3.0 ns. It is found that when the incident flux is represented by the black line (T_{in1}) in Fig. 4(a), the simulated shock velocity (D_{sim1}) is consistent with the experimental result for the whole time. The uncertainty in the incident flux T_{in1} is about 1.2%, which is deduced from the propagation of uncertainty represented by the above equation and the uncertainty in the experimental shock velocity of about 2%. This is also verified by the consistency between the uncertainty in the simulated shock velocity and the experimental results as shown in Fig. 4. The discrepancy between the time-dependent incident fluxes deduced from the flux balance analysis and the shock velocity is small because of the symmetrical and uniform *Hohlraum* design, and the uncertainty in the incident flux from the shock velocity is smaller. Finally, a self-consistent and precise time-dependent radiative albedo with an uncertainty of about 11% is obtained and is compared with the simulated results for different opacity parameters. Compared with the simulation results obtained by using the opacity parameters of THERMOS, those obtained with HYADES are in better agreement with experiments. We have also integrated the reemission flux and incident flux during the laser injection. The efficiency of reemission, given by the ratio of the integrated reemission flux to the integrated incident flux, is about 60%. It is worth noting that about 60% efficiency is a little bit higher than the regularly recognized value of about 40%,[2] since there is no capsule absorption in our cases.

In summary, a self-consistent and precise measurement of the time-dependent radiative albedo for indirect-drive ICF *Hohlraum* wall material has been performed on the SG-100 kJ high power laser facility using a specially designed triple-cavity *Hohlraum*. An approximately constant and near-equilibrium uniform radiation with peak temperature of about 160 eV was created in the secondary cavity. The multi-angle radiative flux of the primary cavity, the reliable reemission flux of the secondary cavity, and the shock velocity of a standard aluminum–quartz sample adhered on the secondary cavity and used to give a credible incident flux were measured. A preliminary time evolution of the radiative albedo and the incident flux for the secondary cavity with large uncertainty were first obtained from the multi-angle flux balance analysis, and then a self-consistent incident flux with small uncertainty was obtained from experimental shock velocity. Finally, a self-consistent and precise measurement of radiative albedo was obtained from the reliable reemission flux and the incident flux with fewer hypotheses and less approximation and was found to agree well with the result of a simulation using the HYADES opacity. Further investigations will be focused on improving the experimental method such through measurement of the reemission flux for the wall material, simultaneous measurement of the reemission flux and shock velocity for the aluminum–quartz sample, and tests of the opacity parameters for more high-Z materials.

The authors would like to thank the target fabrication and laser operation staff for their cooperation. This work was supported by the National Natural Science Foundation of China (Grant No. 12004351).

AUTHOR DECLARATIONS

Conflict of Interest

The authors have no conflicts to disclose.

Author Contributions

Zhiyu Zhang: Conceptualization (equal); Writing – original draft (equal). **Yang Zhao**: Data curation (equal); Supervision (equal). **Xiaoying Han**: Data curation (equal); Supervision (equal). **Liling Li**: Data curation (equal); Validation (equal). **Bo Qing**: Resources (equal); Writing – review & editing (equal). **Lifei Hou**: Resources (equal). **Yulong Li**: Resources (equal). **YuXue Zhang**: Writing – review & editing (equal). **Huan Zhang**: Data curation (equal); Validation (equal). **Xiangming Liu**: Resources (equal). **Bo Deng**: Resources (equal). **Gang Xiong**: Resources (equal). **Min Lv**: Resources (equal). **Tuo Zhu**: Resources (equal). **Chengwu Huang**: Resources (equal). **Tianming Song**: Resources (equal). **Yan Zhao**: Writing – review & editing (equal). **Yingjie Li**: Resources (equal). **Lu Zhang**: Resources (equal). **Xufei Xie**: Supervision (equal). **Jiyan Zhang**: Conceptualization (equal); Supervision (equal); Writing – review & editing (equal). **Jiamin Yang**: Conceptualization (equal); Supervision (equal); Writing – review & editing (equal).

DATA AVAILABILITY

The data that support the findings of this study are available from the corresponding author upon reasonable request.

REFERENCES

[1] J. D. Lindl, "Development of the indirect-drive approach to inertial confinement fusion and the target physics basis for ignition and gain," Phys. Plasmas **2**, 3933 (1995).

[2] J. D. Lindl, P. Amendt, R. L. Berger, S. G. Glendinning, S. H. Glenzer, S. W. Haan, R. L. Kauffman, O. L. Landen, and L. J. Suter, "The physics basis for ignition using indirect-drive targets on the National Ignition Facility," Phys. Plasmas **11**, 339 (2004).

[3] S. Atzeni and J. Meyer-ter Vehn, *The Physics of Inertial Fusion* (Clarendon Press, Oxford, 2004).

[4] H. Abu-Shawareb *et al.*, The Indirect Drive ICF Collaboration, "Achievement of target gain larger than unity in an inertial fusion experiment," Phys. Rev. Lett **132**, 065102 (2024).

[5] T. Ma, P. K. Patel, N. Izumi, P. T. Springer, M. H. Key, L. J. Atherton, L. R. Benedetti, D. K. Bradley, D. A. Callahan, P. M. Celliers, C. J. Cerjan, D. S. Clark, E. L. Dewald, S. N. Dixit, T. Döppner, D. H. Edgell, R. Epstein, S. Glenn, G. Grim, S. W. Haan, B. A. Hammel, D. Hicks, W. W. Hsing, O. S. Jones, S. F. Khan, J. D. Kilkenny, J. L. Kline, G. A. Kyrala, O. L. Landen, S. Le Pape, B. J. MacGowan, A. J. Mackinnon, A. G. MacPhee, N. B. Meezan, J. D. Moody, A. Pak, T. Parham, H.-S. Park, J. E. Ralph, S. P. Regan, B. A. Remington, H. F. Robey, J. S. Ross, B. K. Spears, V. Smalyuk, L. J. Suter, R. Tommasini, R. P. Town, S. V. Weber, J. D. Lindl, M. J. Edwards, S. H. Glenzer, and E. I. Moses, "Onset of hydrodynamic mix in high-velocity, highly compressed inertial confinement fusion implosions," Phys. Rev. Lett. **111**, 085004 (2013).

[6] M. J. Edwards, P. K. Patel, J. D. Lindl, L. J. Atherton, S. H. Glenzer, S. W. Haan, J. D. Kilkenny, O. L. Landen, E. I. Moses, A. Nikroo, R. Petrasso, T. C. Sangster, P. T. Springer, S. Batha, R. Benedetti, L. Bernstein, R. Betti, D. L. Bleuel, T. R. Boehly, D. K. Bradley, J. A. Caggiano, D. A. Callahan, P. M. Celliers, C. J. Cerjan, K. C. Chen, D. S. Clark, G. W. Collins, E. L. Dewald, L. Divol, S. Dixit, T. Doeppner, D. H. Edgell, J. E. Fair, M. Farrell, R. J. Fortner, J. Frenje, M. G. Gatu Johnson, E. Giraldez, V. Y. Glebov, G. Grim, B. A. Hammel, A. V. Hamza, D. R. Harding, S. P. Hatchett, N. Hein, H. W. Herrmann, D. Hicks, D. E. Hinkel, M. Hoppe, W. W. Hsing, N. Izumi, B. Jacoby, O. S. Jones, D. Kalantar, R. Kauffman,

J. L. Kline, J. P. Knauer, J. A. Koch, B. J. Kozioziemski, G. Kyrala, K. N. LaFortune, S. L. Pape, R. J. Leeper, R. Lerche, T. Ma, B. J. MacGowan, A. J. MacKinnon, A. Macphee, E. R. Mapoles, M. M. Marinak, M. Mauldin, P. W. McKenty, M. Meezan, P. A. Michel, J. Milovich, J. D. Moody, M. Moran, D. H. Munro, C. L. Olson, K. Opachich, A. E. Pak, T. Parham, H.-S. Park, J. E. Ralph, S. P. Regan, B. Remington, H. Rinderknecht, H. F. Robey, M. Rosen, S. Ross, J. D. Salmonson, J. Sater, D. H. Schneider, F. H. Séguin, S. M. Sepke, D. A. Shaughnessy, V. A. Smalyuk, B. K. Spears, C. Stoeckl, W. Stoeffl, L. Suter, C. A. Thomas, R. Tommasini, R. P. Town, S. V. Weber, P. J. Wegner, K. Widman, M. Wilke, D. C. Wilson, C. B. Yeamans, and A. Zylstra, "Progress towards ignition on the National Ignition Facility," Phys. Plasmas **20**, 070501 (2013).

[7]D. S. Clark, D. E. Hinkel, D. C. Eder, O. S. Jones, S. W. Haan, B. A. Hammel, M. M. Marinak, J. L. Milovich, H. F. Robey, L. J. Suter, and R. P. J. Town, "Detailed implosion modeling of deuterium-tritium layered experiments on the National Ignition Facility," Phys. Plasmas **20**, 056318 (2013).

[8]J. Lindl, O. Landen, J. Edwards, E. Moses, and NIC Team, "Review of the National Ignition Campaign 2009-2012," Phys. Plasmas **21**, 020501 (2014).

[9]R. P. J. Town, D. K. Bradley, A. Kritcher, O. S. Jones, J. R. Rygg, R. Tommasini, M. Barrios, L. R. Benedetti, L. F. Berzak Hopkins, P. M. Celliers, T. Döppner, E. L. Dewald, D. C. Eder, J. E. Field, S. M. Glenn, N. Izumi, S. W. Haan, S. F. Khan, J. L. Kline, G. A. Kyrala, T. Ma, J. L. Milovich, J. D. Moody, S. R. Nagel, A. Pak, J. L. Peterson, H. F. Robey, J. S. Ross, R. H. H. Scott, B. K. Spears, M. J. Edwards, J. D. Kilkenny, and O. L. Landen, "Dynamic symmetry of indirectly driven inertial confinement fusion capsules on the National Ignition Facility," Phys. Plasmas **21**, 056313 (2014).

[10]T. R. Dittrich, O. A. Hurricane, D. A. Callahan, E. L. Dewald, T. Döppner, D. E. Hinkel, L. F. Berzak Hopkins, S. Le Pape, T. Ma, J. L. Milovich, J. C. Moreno, P. K. Patel, H.-S. Park, B. A. Remington, J. D. Salmonson, and J. L. Kline, "Design of a high-foot high-adiabat ICF capsule for the National Ignition Facility," Phys. Rev. Lett. **112**, 055002 (2014).

[11]H.-S. Park, O. A. Hurricane, D. A. Callahan, D. T. Casey, E. L. Dewald, T. R. Dittrich, T. Döppner, D. E. Hinkel, L. F. Berzak Hopkins, S. Le Pape, T. Ma, P. K. Patel, B. A. Remington, H. F. Robey, J. D. Salmonson, and J. L. Kline, "High-adiabat high-foot inertial confinement fusion implosion experiments on the National Ignition Facility," Phys. Rev. Lett. **112**, 055001 (2014).

[12]J. Gu, Z. Dai, S. Zou, W. Ye, W. Zheng, P. Gu, and S. Zhu, "Effects of mode coupling between low-mode radiation flux asymmetry and intermediate-mode ablator roughness on ignition capsule implosions," Matter Radiat. Extremes **2**, 9 (2017).

[13]K. L. Baker, C. A. Thomas, D. T. Casey, S. Khan, B. K. Spears, R. Nora, T. Woods, J. L. Milovich, R. L. Berger, D. Strozzi, D. Clark, M. Hohenberger, O. A. Hurricane, D. A. Callahan, O. L. Landen, B. Bachmann, R. Benedetti, R. Bionta, P. M. Celliers, D. Fittinghoff, C. Goyon, G. Grim, R. Hatarik, N. Izumi, M. Gatu Johnson, G. Kyrala, T. Ma, M. Millot, S. R. Nagel, A. Pak, P. K. Patel, D. Turnbull, P. L. Volegov, and C. Yeamans, "High-performance indirect-drive cryogenic implosions at high adiabat on the National Ignition Facility," Phys. Rev. Lett. **121**, 135001 (2018).

[14]D. T. Casey, C. A. Thomas, K. L. Baker, B. K. Spears, M. Hohenberger, S. F. Khan, R. C. Nora, C. R. Weber, D. T. Woods, O. A. Hurricane, D. A. Callahan, R. L. Berger, J. L. Milovich, P. K. Patel, T. Ma, A. Pak, L. R. Benedetti, M. Millot, C. Jarrott, O. L. Landen, R. M. Bionta, B. J. MacGowan, D. J. Strozzi, M. Stadermann, J. Biener, A. Nikroo, C. S. Goyon, N. Izumi, S. R. Nagel, B. Bachmann, P. L. Volegov, D. N. Fittinghoff, G. P. Grim, C. B. Yeamans, M. Gatu Johnson, J. A. Frenje, N. Rice, C. Kong, J. Crippen, J. Jaquez, K. Kangas, and C. Wild, "The high velocity, high adiabat, bigfoot campaign and tests of indirect-drive implosion scaling," Phys. Plasmas **25**, 056308 (2018).

[15]A. L. Kritcher, A. B. Zylstra, D. A. Callahan, O. A. Hurricane, C. Weber, J. Ralph, D. T. Casey, A. Pak, K. Baker, B. Bachmann, S. Bhandarkar, J. Biener, R. Bionta, T. Braun, M. Bruhn, C. Choate, D. Clark, J. M. Di Nicola, L. Divol, T. Doeppner, V. Geppert-Kleinrath, S. Haan, J. Heebner, V. Hernandez, D. Hinkel, M. Hohenberger, H. Huang, C. Kong, S. Le Pape, D. Mariscal, E. Marley, L. Masse, K. D. Meaney, M. Millot, A. Moore, K. Newman, A. Nikroo, P. Patel, L. Pelz, N. Rice, H. Robey, J. S. Ross, M. Rubery, J. Salmonson, D. Schlossberg, S. Sepke, K. Sequoia, M. Stadermann, D. Strozzi, R. Tommasini, P. Volegov, C. Wild, S. Yang, C. Young, M. J. Edwards, O. Landen, R. Town, and M. Herrmann, "Achieving record hot spot energies with large HDC implosions on NIF in HYBRID-E," Phys. Plasmas **28**, 072706 (2021).

[16]O. S. Jones, S. H. Glenzer, L. J. Suter, R. E. Turner, K. M. Campbell, E. L. Dewald, B. A. Hammel, J. H. Hammer, R. L. Kauffman, O. L. Landen, M. D. Rosen, R. J. Wallace, and F. A. Weber, "Measurement of the absolute hohlraum-wall albedo under ignition foot drive conditions," Phys. Rev. Lett. **93**, 065002 (2004).

[17]H. Nishimura, H. Takabe, K. Kondo, T. Endo, H. Shiraga, K. Sugimoto, T. Nishikawa, Y. Kato, and S. Nakai, "X-ray emission and transport in gold plasmas generated by 351-nm laser irradiation," Phys. Rev. A **43**, 3073 (1991).

[18]I. B. Földes, K. Eidmann, T. Löwer, J. Massen, R. Sigel, G. D. Tsakiris, S. Witkowski, H. Nishimura, T. Endo, H. Shiraga, M. Takagi, Y. Kato, and S. Nakai, "X-ray reemission from CH foils heated by laser-generated intense thermal radiation," Phys. Rev. E **50**, R690 (1994).

[19]K. Eidmann, I. B. Földes, T. Löwer, J. Massen, R. Sigel, G. D. Tsakiris, S. Witkowski, H. Nishimura, Y. Kato, T. Endo, H. Shiraga, M. Takagi, and S. Nakai, "Radiative heating of low-*Z* solid foils by laser-generated x rays," Phys. Rev. E **52**, 6703 (1995).

[20]R. Sigel, G. Tsakiris, F. Lavarenne, J. Massen, R. Fedosejevs, K. Eidmann, J. Meyer-ter Vehn, M. Murakami, S. Witkowski, H. Nishimura *et al.*, "Experimental investigation of radiation heat waves driven by laser-induced Planck radiation," Phys. Rev. A **45**, 3987 (1992).

[21]Z. Wanguo, Z. Xiaomin, W. Xiaofeng, J. Feng, S. Zhan, Z. Kuixin, Y. Xiaodong, J. Xiaodong, S. Jingqin, Z. Hai, L. Mingzhong, W. Jianjun, H. Dongxia, H. Shaobo, X. Yong, P. Zhitao, F. Bin, G. Liangfu, L. Xiaoqun, Z. Qihua, Y. Haiwu, Y. Yong, F. Dianyuan, and Z. Weiyan, "Status of the SG-III solid-state laser facility," J. Phys.: Conf. Ser. **112**, 032009 (2008).

[22]W. Zheng, X. Wei, Q. Zhu, F. Jing, D. Hu, X. Yuan, W. Dai, W. Zhou, F. Wang, D. Xu, X. Xie, B. Feng, Z. Peng, L. Guo, Y. Chen, X. Zhang, L. Liu, D. Lin, Z. Dang, Y. Xiang, R. Zhang, F. Wang, H. Jia, and X. Deng, "Laser performance upgrade for precise ICF experiment in SG-III laser facility," Matter Radiat. Extremes **2**, 243 (2017).

[23]X. Xie, H. Du, J. Chen, S. Liu, Z. Li, D. Yang, Y. Huang, K. Ren, L. Hou, S. Li, L. Guo, X. Jiang, W. Huo, Y. Chen, G. Ren, K. Lan, F. Wang, S. Jiang, and Y. Ding, "Application of the space-resolving flux detector for radiation measurements from an octahedral-aperture spherical hohlraum," Rev. Sci. Instrum. **89**, 063502 (2018).

[24]F. Wang, X. Peng, S. Liu, T. Xu, L. Mei, X. Jiang, and Y. Ding, "A line-imaging velocity interferometer technique for shock diagnostics without x-ray preheat limitation," Rev. Sci. Instrum. **82**, 103108 (2011).

[25]L. Jing, S. Jiang, D. Yang, H. Li, L. Zhang, Z. Lin, L. Li, L. Kuang, Y. Huang, and Y. Ding, "Angular radiation temperature simulation for time-dependent capsule drive prediction in inertial confinement fusion," Phys. Plasmas **22**, 022709 (2015).

[26]Z. Li, X. Jiang, S. Liu, T. Huang, J. Zheng, J. Yang, S. Li, L. Guo, X. Zhao, H. Du, T. Song, R. Yi, Y. Liu, S. Jiang, and Y. Ding, "A novel flat-response x-ray detector in the photon energy range of 0.1–4 keV," Rev. Sci. Instrum. **81**, 073504 (2010).

[27]S. Tianming, Y. Jiamin, and Y. Rongqing, "Recover soft x-ray spectrum using virtual flat response channels with filtered x-ray diode array," Rev. Sci. Instrum. **83**, 113102 (2012).

[28]L. Guo, X. Li, X. Xie, B. Deng, X. Jiang, S. Li, Z. Li, K. Deng, Q. Wang, Z. Cao, P. Song, H. Du, Y. Yang, X. Che, L. Hou, W. Zha, T. Xu, S. Liu, C. Zheng, W. Zheng, Y. Ding, D. Yang, F. Wang, J. Yang, S. Jiang, and B. Zhang, "Experimental and simulation studies on gold bubble movement in gas-filled hohlraums," Nucl. Fusion **59**, 016002 (2019).

[29]L. Guo, S. Li, J. Zheng, Z. Li, D. Yang, H. Du, L. Hou, Y. Cui, J. Yang, S. Liu *et al.*, "A compact flat-response x-ray detector for the radiation flux in the range from 1.6 keV to 4.4 keV," Meas. Sci. and Technol. **23**, 065902 (2012).

[30]R. E. Olson, D. K. Bradley, G. A. Rochau, G. W. Collins, R. J. Leeper, and L. J. Suter, "Time-resolved characterization of *Hohlraum* radiation temperature via interferometer measurement of quartz shock velocity," Rev. Sci. Instrum. **77**, 10E531 (2006).

[31]R. Ramis, R. Schmalz, and J. Meyer-Ter-Vehn, "MULTI—A computer code for one-dimensional multigroup radiation hydrodynamics," Comput. Phys. Comm. **49**, 475 (1988).

[32]W. Liu, X. Duan, S. Jiang, Z. Wang, L. Sun, H. Liu, W. Yang, H. Zhang, Q. Ye, P. Wang, Y. Li, L. Yi, and S. Dong, "Laser-driven shock compression of gold foam in the terapascal pressure range," Phys. Plasmas **25**, 062707 (2018).

[33]C. Zhang, H. Liu, X. Duan, Y. Liu, H. Zhang, L. Sun, Q. Ye, W. Yang, F. Wang, J. Yang, S. Jiang, Z. Wang, and Y. Ding, "Study of M-band X-ray preheating effect on shock propagation via streaked optical pyrometer system at SG-III prototype lasers," Phys. Plasmas **26**, 012708 (2019).
[34]X. Duan, C. Zhang, Z. Guan, L. Sun, X. Peng, H. Liu, W. Yang, Y. Li, H. Zhang, Q. Ye, J. Yang, S. Jiang, and Z. Wang, "Transparency measurement of lithium fluoride under laser-driven accelerating shock loading," J. Appl. Phys. **128**, 015902 (2020).
[35]P. Wang, C. Zhang, S. Jiang, X. Duan, H. Zhang, L. Li, W. Yang, Y. Liu, Y. Li, L. Sun, H. Liu, and Z. Wang, "Density-dependent shock Hugoniot of polycrystalline diamond at pressures relevant to ICF," Matter Radiat. Extremes **6**, 035902 (2021).